Ambika, S. et al.

Article

Structural, morphological and optical properties and solar cell applications of thioglycolic routed nano cobalt oxide material

Energy Reports

Provided in Cooperation with:
Elsevier

Suggested Citation: Ambika, S. et al. (2019) : Structural, morphological and optical properties and solar cell applications of thioglycolic routed nano cobalt oxide material, Energy Reports, ISSN 2352-4847, Elsevier, Amsterdam, Vol. 5, pp. 305-309, https://doi.org/10.1016/j.egyr.2019.02.005

Energy Reports 5 (2019) 305–309

Contents lists available at ScienceDirect

Energy Reports

journal homepage: www.elsevier.com/locate/egyr

Research paper

Structural, morphological and optical properties and solar cell applications of thioglycolic routed nano cobalt oxide material

S. Ambika [a,b,*], S. Gopinath [a,c], K. Saravanan [d], K. Sivakumar [e], C. Ragupathi [f], T.A. Sukantha [g,**]

[a] Research and Development Centre, Department of Chemistry, Bharathiar University, Coimbatore 641046, India
[b] Department of Chemistry, M.Kumarasamy College of Engineering, Karur 639113, India
[c] Department of Chemistry, Chettinad College of Engineering & Technology, Karur 639114, India
[d] Department of Chemistry, Thiruvalluvar Government Arts College, Rasipuram 637401, India
[e] Department of Chemistry, Adhiyamaan College of Engineering, Hosur, 635109, India
[f] Department of Chemistry, Sriram College of Arts & Science, Thiruvallur 602024, India
[g] Department of Chemistry, K.S. Rangasamy College of Technology, Tiruchengode 637215, India

HIGHLIGHTS

- A novel synthesis method is presented for Co_3O_4
- Nanomaterial with controlled crystallite size.
- Only fuels with different morphologies formation.

GRAPHICAL ABSTRACT

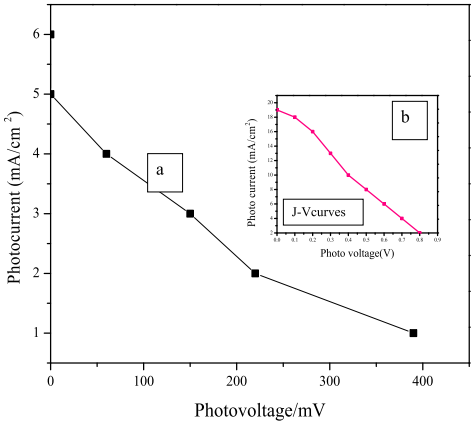

Fig. a. Photocurrent-voltage curves of cobalt oxide DSSC and Fig. b. J–V characteristics of DSSCs using cobalt oxide

ARTICLE INFO

Article history:
Received 12 May 2018
Received in revised form 1 November 2018
Accepted 14 February 2019
Available online xxxx

Keywords:
Hydrothermal
Structure
Morphology
DSSC and nano

ABSTRACT

In this research, cobalt oxide produced by the hydrothermal method through the using thioglycolic acid (TGA) as the fuel is discussed in this paper. The produced cobalt oxide nanomaterials are characterized via X-ray diffraction analysis (XRD), high resolution scanning electron microscopy (HR-SEM), high resolution transmission electron microscopy (HR-TEM), diffuse reflectance spectroscopy (DRS). Additionally, as a possible promising application of the cobalt oxide based dye-sensitized solar cells (DSSCs) are successfully fabricated and the cell performances are evaluated. Solar cells have recently drawn a growing research interest due to their increasing power conversion efficiency, proper bandgap, high absorption coefficient and the earth abundant nature.

* Corresponding author at: Department of Chemistry, M.Kumarasamy College of Engineering, Karur 639113, India.
** Corresponding author.

E-mail addresses: ambika0022@gmail.com (S. Ambika), sukanthachem2017@gmail.com (T.A. Sukantha).

https://doi.org/10.1016/j.egyr.2019.02.005

1. Introduction

Transition-metal oxides [TMOs] have been found place in many research areas due to their exclusive properties, such as, semiconducting behavior, spin-polarization, magnetic, optical, solar cells and antibacterial activity. Intensive research is presently being carried out on enhancing these properties and the adding novel functionalities to the oxides (Søndenå et al., 2007). In recent years, development of solar cells that the directly convert sun light into electricity. Solar cell is one of the most promising technologies for collecting that the sun energy as the largest non-carbon and carbon based natural source. Photovoltaic acceptance has been growing to present in satisfactory for alternatives to the conventional solar cells. Solar cells, that the lowest cost and the simplest fabrication method for solar cells is solution processing that provides roll-to-roll printing as a beneficial method for large scale production. In recent years, Fuel cells have advantages over other systems because of their high electrical efficiency and fuel flexibility. Several type of fuel cell requires specific materials and the fuels for different applications. Recent advances, fuel cell types, such as, alkaline fuel cells (AFCs), molten carbonate fuel cells (MCFCs) and solid oxide fuel cells (SOFCs). Currently, researchers focus on SOFCs. SOFCs have many advantages for a wide range of applications because of their electrical efficiency, potential to use natural gas, biogas or CH_4 as a fuel and high performance. Solid oxide fuel cells (SOFCs) are considered as a highly encouraging way for green electric power generation from fossil fuels and the renewable energy with much fewer impressions on the environment. It is the key to develop new cathode with excellent electro-catalytic activity toward the oxygen reduction reaction (ORR) within the intermediate temperature range, as it is the limitation for the total polarization (Zhu et al., 2016). The most important factor influencing fuel cell performance is the material used as a catalyst. Catalysts speed up the reactions at both anode and cathode. There are several types of fuel cells. They are categorized depending on the nature of the electrolyte (Brousse et al., 2015). Nowadays, that the challenges associated with up conversion of sub-bandgap photons lie in both the solar cell technology and the up converter material side.

Various synthetic approaches for cobalt oxide based nanomaterials are being developed in the last few years with respect to achieving control of crystallite size, shape, and assembly behavior (Gogotsi and Penner, 2018). Spinel-type cobalt oxide (Co_3O_4) is commonly prepared by the ceramic technique that the involves, combustion method (Bilecka et al., 2008), or microwave irradiation (Jiu et al., 2002), or hydrothermal/solvothermal method (Gu et al., 2007) or chemical spray pyrolysis (Gardey-Merino et al., 2012), or sonochemical method (Ai and Jiang, 2009) and modified sol–gel method (Li and Ren, 2006). New fuel based methods has been developed as a mild hydrothermal method to synthesize cobalt oxides by the using thioglycolic acid (TGA). We have presented here a hydrothermal method, which is milder, simpler, and more environmental friendly than other methods. The unique advantage of this method is inexpensive raw materials and simple preparation process. Therefore, it is possible to control both kinetic and thermodynamic factors of the preparation using hydrothermal method (Sharma et al., 2010).

Currently, that the efficiently of engineer the cobalt oxide surfaces/interfaces; the quest to find an optimal and the champion passivating material that can efficiently improve the cobalt oxide solar cell performance is appealing and the success could be much reliant on the understanding of the structures and the properties of the passivating layer/ cobalt oxide system. In recent years, efforts should be spent on elucidating the mechanisms of passivating layer effects on the cobalt oxide solar cell performance. A number of efforts have been made to minimize that the two major losses occurring in single junction solar cells i.e., the sub band gap transmission and thermalization of hot carriers (Schouwink et al., 2014). To the best of our consent, we mainly research work, the progress and achievements in the preparation processes. Finally, we outline the challenges and the perspectives of this promising solar cell.

2. Materials and methods

2.1. Preparation of Co_3O_4

Analytical grade $Co(NO_3)_2.6H_2O$ from Sigma–Aldrich company with minimum purity of 99 wt.% as received, and thioglycolic acid (TGA) from Sigma Aldrich company, 99.5 wt.%, were used as starting materials. A mixed solution of cobalt nitrate [1 M] is dissolved in 100 ml distilled water and 100 ml 0.08 M of thioglycolic acid (TGA) was mixed slowly under stirring. After stirring, the reactants were put into a 250 ml capacity Teflon-lined autoclave. The autoclave was maintained at 100–160 °C for 5–7 h and then cooled down to room temperature naturally. The product was centrifuged, washed with alcohol and distilled water for several times, and dried in the air at 120 °C for 5 h.

2.2. Characterization of cobalt oxide

Cobalt oxide chemical analysis was analyzed by a Scanning Electron Microscope (SEM) model, CARL ZEISS EVO MA15. The structural studies on cobalt oxide nanoparticles were done using Seifert 3003 TT X-ray diffractometer with Cu Kα radiation with a wavelength of 1.540 Å and the system was operated at 30 keV in a scan range of 20–100° Phillips TECHNAI FE 12. Stereo-scan LEO 440 and a high resolution transmission electron microscope (HR-TEM). Diffuse reflectance measurements were performed by Jasco V-670 double-beam spectrometer for energy gap determination.

2.3. Fabrication of solar cells

The cobalt oxide was used as photo-anodes in DSSCs with a 3-mm thickness, sensitized in a 0.03 mM acetone solution of Ruthenium (II) cis-di(thiocyano) bis (2,2′-bypyr-idyl-4,4'dicarboxylic acid) (N_3) dyes for at least 10 h at 50 °C. The excess unanchored dyes were rinsed off using absolute acetone and dried in air, then the covered with platinum sheet as counter electrodes. The internal space of the cell was filled with liquid electrolyte (0.3 M LiI, 0.03 M I_2) dissolved in acetonitrile by the capillary action. The photovoltaic characteristics were measured by 614 Keithley picoammeter under Oriel solar simulator illumination (AM1.5, 100 mW/cm^2).

3. Results and discussion

XRD analysis supplies the width and the intensity of the diffraction peaks is depending on lattice strain, crystallite size, and other imperfections, such as, stacking responsibilities. The XRD patterns of cobalt oxide nanoparticles are shown in Fig. 1. 2θ values at 24.53°, 27.25°, 31.30°, 36.99°, 44.97°, 49.56°, 55.14°, 59.78°, 65.90°, and 77.12° appeared. XRD analysis supplies the width and the intensity of the diffraction peaks is contingent on lattice strain, crystallite size, and other imperfections, such as, stacking responsibilities. The XRD patterns of cobalt oxide nanoparticles are shown in Fig. 1. 2θ values at 31.30°, 36.99°, 44.97°, 49.56°, 55.14°, 59.78°, and 65.90°, appeared. (220), (311), (222), (400), (331), (511) and (440) crystal planes of the cubic spinel structure, respectively. Cobalt oxides presented in diffraction peak positions, inter planar distanced (Å) values of (FWHM) full-width at half-maximum, [1.0012], [0.9345], [1.0967], [1.3467],

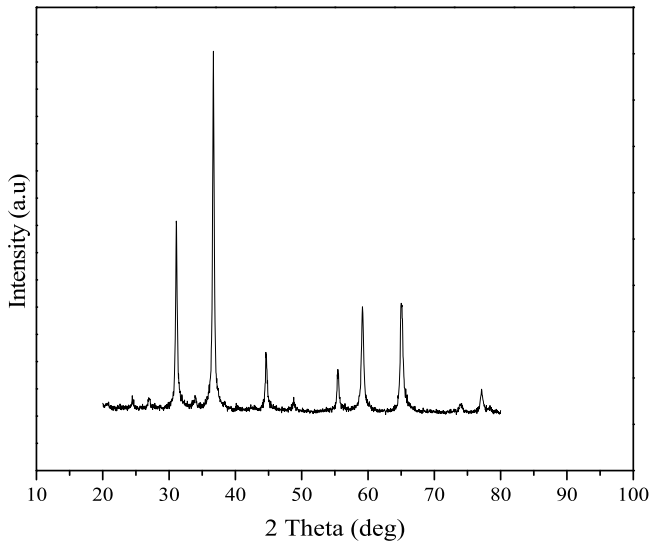

Fig. 1. XRD pattern of cobalt oxide prepared by Hydrothermal method.

[1.4744], [1.0242] and [1.2287], respectively. These diffraction peaks are indexed to the crystalline cubic phase of Co_3O_4 with lattice constants of a = 8.076 Å and a space group of Fd3 m, which are in agreement with the reported values (JCPDS card no. 76-1802). These diffraction peaks are indexed to the crystalline cubic phase of Co_3O_4 with lattice constants of a = 8.076 Å and a space group of Fd_3 m, which are in consent with the reported values (JCPDS card no. 76–1802).

The average crystallite size is obtained from XRD peaks using Scherrer equation (Becheri et al., 2008).

$$L = \frac{0.89\lambda}{\beta \cos\theta}$$

where, L = average crystallite size (Å), λ = wavelength of the incident X-ray beam (1.54 Å), β = the FWHM (rad), and θ = Bragg's angle. The average crystallite size for the sample was found to be 17.2 nm, respectively.

By SEM analysis it is observed that the Co_3O_4 exhibited a high degree of agglomeration, as is shown in Fig. 2(a, b). The EDX result showed (Fig. 2c) the presence of Co_3O_4 by the appearance of Co and O peaks in the spectrum. Though, the presence of cobalt oxides no impurity is also evidenced from the EDX spectrum.

A comparable agglomeration is evidenced in Co_3O_4 powders synthetized by synthesis using thioglycolic acid (TGA) as fuel. Fig. 3(c, d) is the TEM image of the cobalt oxide nanopowder. It shows the formation of the agglomerated spherical shaped nanoparticles. The average crystal size observed from XRD is considerably small compared to the mean size calculated from TEM particle size histograms. Nonetheless, a more rapidly appearance arguments available that the particle size represented by the mean intensity peaks form maximum peak obtained XRD spectra (crystal region) is a considerable agreement with the mean size calculated from the TEM measurement in visible region (particle size for tiny particles into present in agglomerated/ aggregates) within acceptable error limit for present instrumentation. Co_3O_4 nanoparticle (interaction for Co-O) means that the outstanding to the micro-nano motions for nanoparticle, that the atoms in the nano sized metal oxides are more active than those of the base metal oxides in preparation method (Bindu and Thomas, 2014; Paul et al., 2010). In hydrothermal process the decomposition of the precursors at a specific flush depends on the temperature and pressure inside the reaction container. Now, pressure is related to the fraction of the solvent and is kept constant for all the experiments. Initially synthesis is achieved in water with in concentrations of thioglycolic acid (TGA). Synthesis is carried out in different experimental conditions to get the optimum condition for the formation of Co_3O_4 based nanoparticles.

The fundamental absorption, which agrees to the conversion from valence to the conduction band, can be used to regulate the band gap energy of the oxide material. For analysis purposes, the diffuse-reflectance (R) of the sample can be related to the Kubelka–Munk function F(R) by the relation $F(R)=(1-R)^2/2R$ (He et al., 2005). The optical property of the cobalt oxide is considered by the DRS in the UV–Vis region. Fig. 4a shows the DRS spectra recorded at room temperature in the wavelength choice of 200–800 nm. From this spectra, it may be observed that the absorption edge of the Co_3O_4 is slightly shifted (350–550) to lower wavelength with increasing Co^{3+} concentration. The first band (200–300) is assigned to the $O^{2-} \rightarrow Co^{2+}$charge transfer process while the second band (350–700) is assigned to the $O^{2-} \rightarrow Co^{3+}$charge transfer (Subba Ramaiah et al., 2001). Present work, that the bandgap energies are (Fig. 4b) 4.10 eV for the Co_3O_4 nanoparticles. The increases in the optical band gap energy exhibitions an increasing trend as the particle size decreases due to the quantum confinement of cobalt oxides. the nanoparticles influence the optical devices (Ramamoorthy and Rajendran, 2017).

Fig. 5a shown the photocurrent–voltage curve of the DSSCs obtained with the 2-mm cobalt oxide. During the photocurrent measurements, the cell efficiency (h) is expressed by the following equation:

$$\eta = (V_{oc}J_{sc}FF)/P_{in} \quad (1)$$

$$FF = V_{opt}J_{opt}/V_{oc}J_{sc} \quad (2)$$

Which P in is the power of white light, FF is fill factor, V_{opt} and J_{opt} are voltage and current for determined power output, and V_{oc} and J_{sc} are open-circuit photovoltage and short-circuit photocurrent, respectively. The cell effectiveness, small circuit current and the open-circuit photovoltage of cobalt oxide DSSC is 1.3%, 5.10 mA cm^{-2} and 397 mV, respectively (Peh et al., 2010). Present work, J–V curves of the fabricated DSSCs sensitized by the N719 under standard AM 1.5 illumination (100 Ma/cm^{-2}) are shown in Fig. 5b. The detailed values for photovoltaic parameters of all devices, including the short-circuit photocurrent density J_{sc}(mA/cm^2) 19.02 ± 0.21, open-circuit voltage (V_{oc}) 0.812 ± 0.008, fill factor (FF) 0.69 ± 0.09 and PCE % (9.05 ± 0.02) are collected in cobalt oxides. Cobalt oxides aggregated have been effectively decreased the surface area, and with direct contact to the dye molecules, it resulted in a lower amount of adhered dye molecules to convert sunlight thereby leading to a lower J_{sc} (Peter and Wijayantha, 1999).

Fig. 6 shows the XPS spectra of Co_3O_4, the binding energy of $Co^{3+}2p_{3/2}$ electrons on for 782 eV and $Co^{2+}2p_{1/2}$ for 797 eV. The relative ratio of Co $_{2þ}$ to Co $_{3þ}$ can be assessed by calculating the corresponding integrated areas. The binding energy shifts about to a lower value, indicating the (Co^{2+}–O^-) bond in (Co^{3+}–O^-) high value indicated for Co_3O_4. As suggested by the mechanism, as follows

$$2Co^{3+} - O^- \rightarrow Co^{3+} - O - O - Co^{3+} \rightarrow O_2 + 2Co^{2+}$$

To extend the in above mechanism, it is assumed that the two adsorbed oxygen atoms (Co^{3+}–O—) produced. The bond energies of these peaks are very consistent with the $Co^{3+}$and Co^{2+}cations reported in previous literature of Co_3O_4 (Zhang et al., 2016; Kumar et al., 2016).

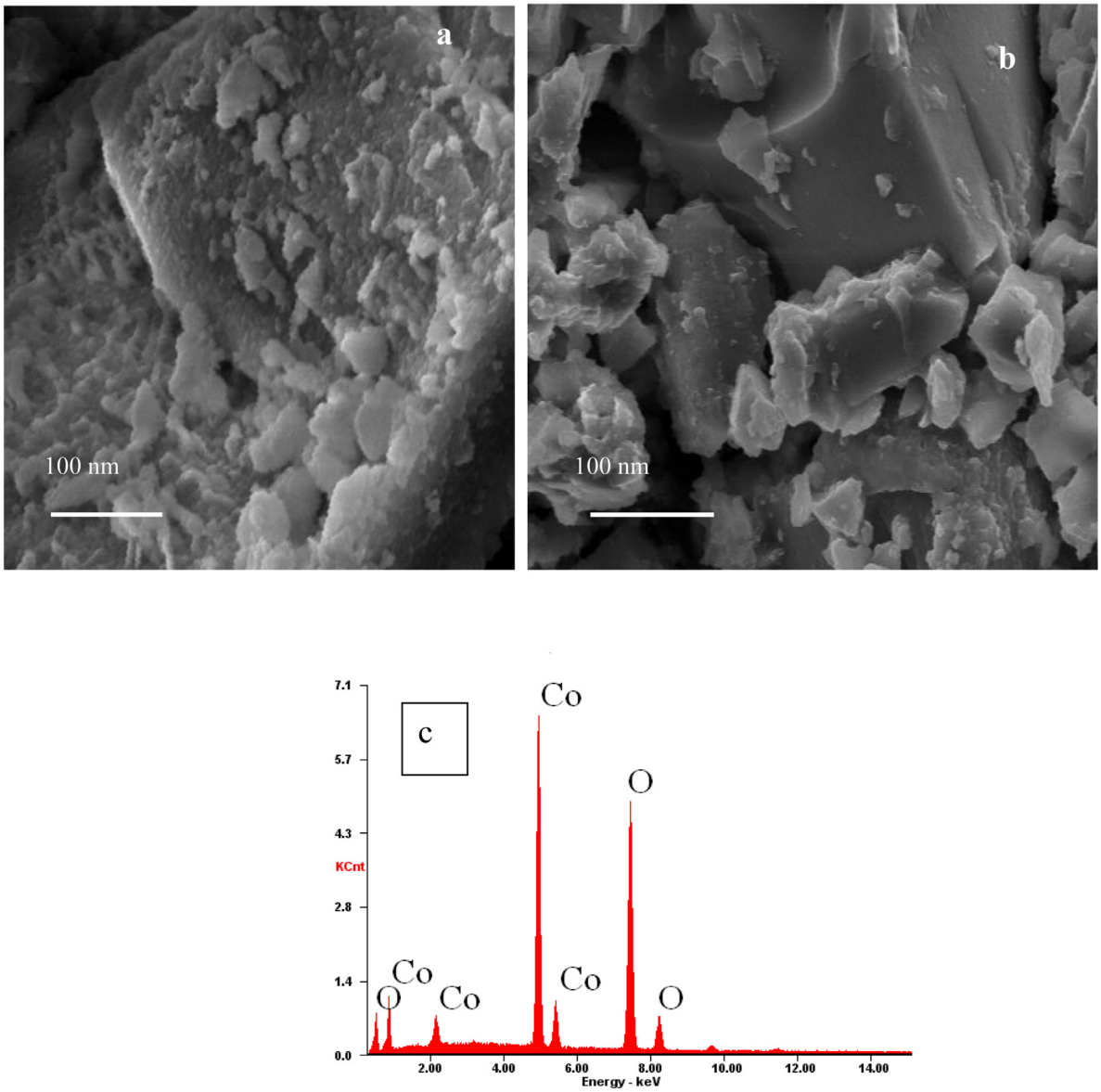

Fig. 2. (a,b) SEM pattern of cobalt oxide prepared by Hydrothermal method. (c) EDS spectrum of cobalt oxide.

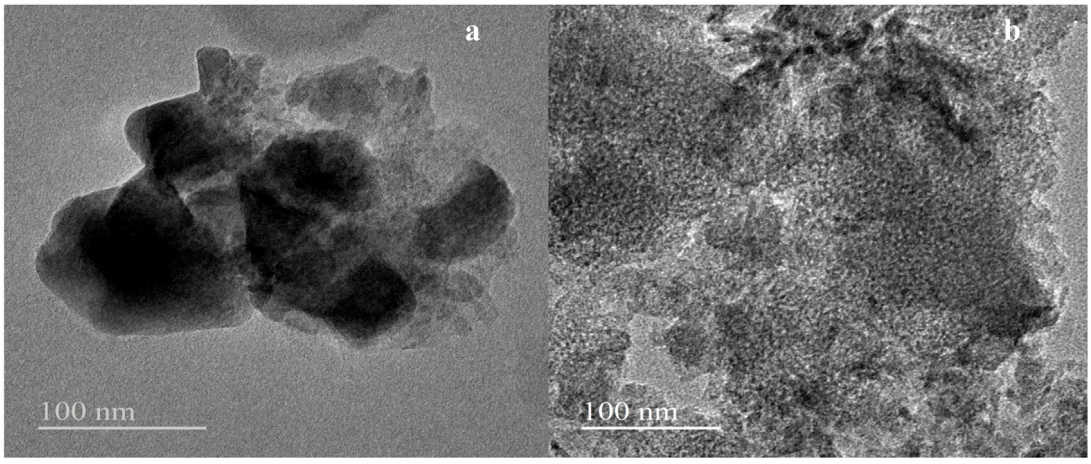

Fig. 3. (a,b) TEM pattern of cobalt oxide prepared by Hydrothermal method.

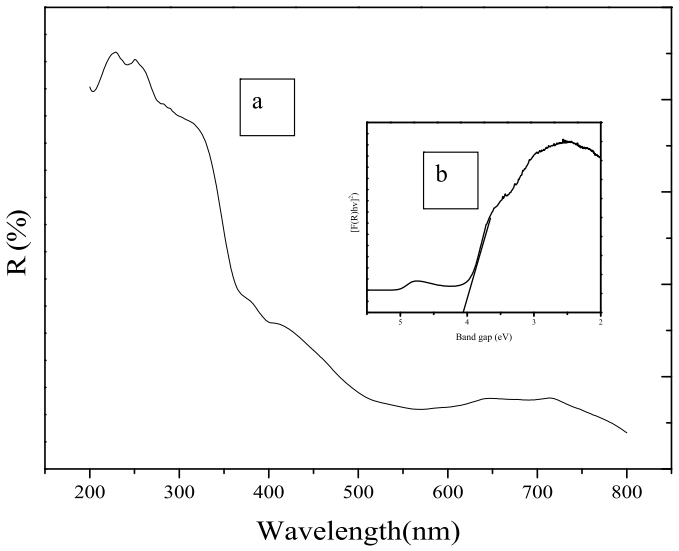

Fig. 4. (a) Diffuse reflectance spectra of cobalt oxide prepared by Hydrothermal method. (b) Bandgap energy for of cobalt oxide.

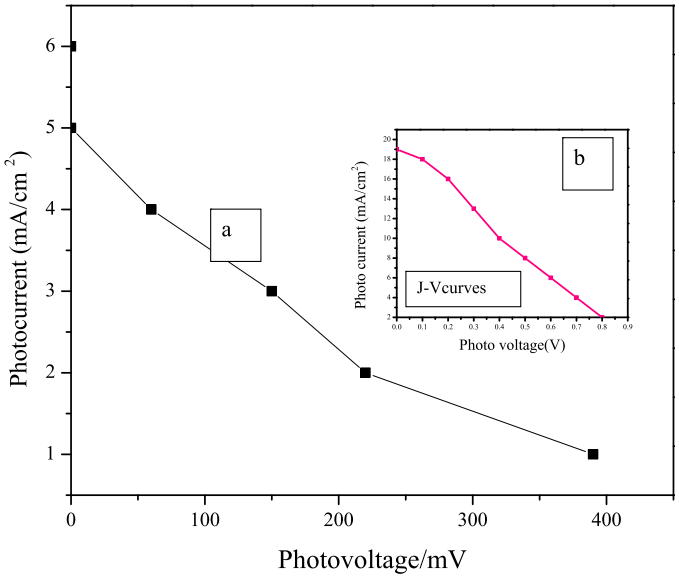

Fig. 5. (a) Photocurrent–voltage curves of cobalt oxide DSSC. (b) J–V characteristics of DSSCs using cobalt oxide.

4. Conclusion

The Co_3O_4 is well-dispersed with high crystallinity, terms of size, morphology, optical and the Co_3O_4 particles thereby leading to high solar cell efficiency. Experimental design and analysis of cobalt oxide based DSSC is carried out. Thus in the present study we explained an improved DSSC constructed with hydrothermally synthesized cobalt oxide. In addition, hydrothermal method

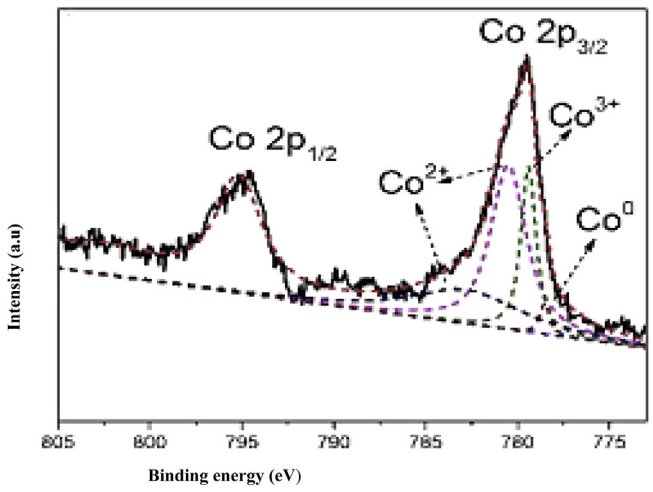

Fig. 6. XPS spectrum for cobalt oxide.

is very simple, inexpensive and energy efficient to obtain Co_3O_4 materials in nanoscale range. Therefore, Co_3O_4nanoparticles in the large area processes are a positive step for the development of low-cost antireflection and are a good choice for the easy low temperature fabrication solar cells as well as environmental friendly deposition methods.

References

Ai, L.-H., Jiang, J., 2009. Powder Tech. 195, 11–14.
Becheri, A., Durr, M., Nostro, P.L., Baglioni, P., 2008. J. Nanopart. Res. 10, 679–689.
Bilecka, I., Djerdj, I., Niederberger, M., 2008. Chem. Commun. 886–888.
Bindu, P., Thomas, S., 2014. J. Theor. Appl. Phys. 8, 123–134.
Brousse, T., Belanger, D., Long, J.W., 2015. J. Electrochem. Soc. 162, A5185–A5189.
Gardey-Merino, M.C., Palermo, M., Belda, R., Fernández De Rapp, M.E., Lascalea, G.E., Vázquez, P.G., 2012. Proc. Mater. Sci. 1, 588–593.
Gogotsi, Y., Penner, R.M., 2018. ACS Nano 12, 2081–2083.
Gu, F., Li, C., Hu, Y., Zhang, L., 2007. J. Cryst. Growth 304, 369–373.
He, T., Chen, D.R., Jiao, X.L., Wang, Y.L., Duan, Y.Z., 2005. Chem. Mater. 17, 4023–4030.
Jiu, J., Ge, Y., Li, X., Nie, L., 2002. Mater. Lett. 54, 260–263.
Kumar, K., Canaff, C., Rousseau, J., Arrii-Clacens, S., Napporn, T.W., Habrioux, A., Kokoh, K.B., 2016. J. Phys. Chem. C 120, 7949–7958.
Li, L., Ren, J., 2006. Mater. Res. Bull. 41, 2286–2290.
Paul, G., Pal, T., Manna, I., 2010. J. Colloid Interface Sci. 349, 434–437.
Peh, C.K.N., KE, L., Ho, G.W., 2010. Mater. Lett. 64, 1372–1375.
Peter, L.M., Wijayantha, K.G., 1999. Electrochem. Commun. 1, 576–580.
Ramamoorthy, C., Rajendran, V., 2017. Optik 145, 330–335.
Schouwink, P., Ley, M.B., Tissot, A., Hagemann, H., Jensen, T.R., Smrčok, Ľ., Černý, R., 2014. Nature Commun. 5, 5706.
Sharma, D., Rajput, J., Kaith, B.S., Kaur, M., Sharma, S., 2010. Thin Solid Films 519, 1224–1229.
Søndenå, Rune, Stølen, Svein, Ravindran, P., Grande, Tor, Allan, Neil L., 2007. Phys. Rev. B 75, 184105.
Subba Ramaiah, K., Pilkington, R.D., Hill, A.E., Tomlinson, R.D., Bhatnagar, A.K., 2001. Mater. Chem. Phys. 68, 22–30.
Zhang, C., Xiao, J., Lv, X., Qian, L., Yuan, S., Wang, S., Lei, P., 2016. J. Mater. Chem. A 4, 16516–16523.
Zhu, Y., Zhou, W., Ran, R., Chen, Y., Shao, Z., Liu, M., 2016. Nano Lett. 16, 512–518.